| | |
|---|---|
| **Preprint Title** | Identification of the physical-chemical properties that modulate the nanoparticles aggregation in blood |
| **Authors** | Ludovica Soddu, Duong N. Trinh, Eimear Dunne, Dermot Kenny, Giorgia Bernardini, Ida Kokalari, Arianna Marucco, Marco P. Monopoli and Ivana Fenoglio |
| **Publication Date** | 01 Okt 2019 |
| **Article Type** | Full Research Paper |
| **Supporting Information File 1** | SI.docx;  1.3 MB |
| **ORCID® iDs** | Ludovica Soddu - https://orcid.org/0000-0001-6675-2318; Dermot Kenny - https://orcid.org/0000-0001-5548-3263; Ida Kokalari - https://orcid.org/0000-0003-0859-1354; Marco P. Monopoli - https://orcid.org/0000-0002-2035-6894; Ivana Fenoglio - https://orcid.org/0000-0002-6946-3105 |

# Identification of the physical-chemical properties that modulate the nanoparticles aggregation in blood

Ludovica Soddu[a,b], Duong N. Trinh [c], Eimear Dunne[b], Dermot Kenny[b], Giorgia Bernardini[a,c], Ida Kokalari[a], Arianna Marucco[a], Marco P Monopoli[c] * and Ivana Fenoglio[a]*.

[a]Department of Chemistry, University of Torino, 10125 Torino, Italy
[b]Molecular and Cellular Therapeutics, Royal College of Surgeons in Ireland, Dublin, Ireland.
[c]Department of Chemistry, Royal College of Surgeons in Ireland, Dublin, Ireland

Correspondent Authors:

Ivana Fenoglio; ivana.fenoglio@unito.it

Marco Monopoli; marcomonopoli@rcsi.ie

## Abstract

Inorganic materials are receiving significant interest in medicine given their usefulness for therapeutic applications such as targeted drug delivery, carriers of active pharmaceutical and medical imaging. However, the poor knowledge of the side effects related to their use is an obstacle to their clinical translation. For the molecular drug development, safe-by-design has become as a novel pharmaceutical strategy that allows a reduction of the costs and an acceleration of the translation of research to market. In the case of materials, the application of such approaches is hampered by a poor knowledge of how the physical and chemical properties of the material trigger biological response. Hemocompatibility is a crucial factor for those materials that are intended for medical applications. In particular, the formation of agglomerates is a serious side effect that may induce occlusion of blood vessels and thrombotic events. Additionally, nanoparticles can interfere with the coagulation cascades where they have been reported to induce both pro- and anti-coagulant properties where their properties like size, shape and surface charge have been see to be critical parameters.

Here, we developed two sets of tailored carbon and silica nano/submicron-particles with three different sizes (100-500 nm) with the purpose of investigating the role of surface curvature and chemistry on platelet aggregation, activation and adhesion.

We show that that large carbon nanoparticles, but not small carbon nanoparticles or silica nanoparticles, have a strong tendency to form aggregates both in plasma and blood, as a consequence of the formation of a protein corona and not of platelets activation. Substantial differences were found in the composition of the protein corona depending upon the chemical nature of the nanoparticles, while the surface curvature plays a minor role. On the other hand, coagulation proteins were abundant in the corona of both silica and carbon nanoparticles.

The results presented herein suggest that vessel occlusion and formation of thrombi in vivo may occur through independent mode of action (MoA), differently affected by the physico-chemical properties of the materials.

**Keywords:** platelets aggregation, nanoparticles, aggregation, size, surface chemistry

## 1.    Introduction

Nanomedicine is probably one of the most exciting field of research in the branch of nanotechnology as it has the potential to solve practical and effective solution on several diseases where traditional drugs currently fail. However, a tremendous gap exists between the number of formulations proposed and those approved for clinics [1]. Among the several factors that hampers the translation process, the most critical ones are the batch-to-batch variability and the poor knowledge of the properties modulating nanomaterial efficacy and safety [2].

Safe-by-design (SbD) approach has a great potential in accelerating the entrance of medicines into market [3], reducing pre-clinical research and costs. However, a deep knowledge of the processes leading to the adverse effects and of the physico-chemical properties governing such processes are mandatory to build structure-activity relationships (SARs) that in turn enable the SbD approaches.

To the latter aspect, knowledge may only be derived by collecting a substantial amount of data from libraries of nanomaterials with definite synthetic properties.

Therefore, understanding the processes that occur in the bloodstream are particularly relevant, not only for nanoformulations administered by intravenous injection, but also for any material introduced into the body.

Nanoparticles have been found to be able of promoting both haemorrhage or thrombosis [4,5], by interfering with the coagulation system through different pathways. Depletion of soluble coagulation factors (e.g fibrinogen, XII factor) may occur following adsorption of the factors at the surface of the nanoparticles. On the other hand, activation of some factors by surface-driven exposure of cryptic domains following adsorption was reported in some studies. Other studies reported the ability of nanoparticles to damage or activate platelets, endothelial cells or monocytes [5].

Physico-chemical properties were found to be critical in determining the ability of the materials to induce adverse effects. Several studies focused on the effect of surface charge and particle size. Albeit such properties were shown to clearly affect the pro-anticoagulant activity of nanoparticles, the direction of the effect varies, depending on the kind of material. For example, positive charged dendritic nanoparticles were found to be more thrombogenic than negatively charged while for polystyrene nanoparticles both positive and negative charged surfaces were found to induce platelet activation [6,7]. These differences are likely due to the coexistence of different molecular processes, but also to the combined effect of different physico-chemical properties.

Due to their promising properties, carbon and silica nanoparticles are among the most studied inorganic materials for medical applications. Their ability to induce thrombus formation, along with their mechanisms of action, is still under debate.

Both single-walled carbon nanotubes (SWCNTs) and multiwalled carbon nanotubes (MWCNTs) were found to induce platelet activation [8,9] by perturbing $Ca^{2+}$ homeostasis, an effect that was hypothesized to be caused by the interaction of CNT with plasma and dense tubular system membranes likely related to the fibrous shape [10]. On the other hand, contrasting data have been reported on the potential of isometric carbon nanoparticles like carbon black, fullerenes and diesel

exhaust to induce platelet activation and aggregation [8,9,11]. Systemic administration of carbon black in mice resulted in fibrinogen and platelet deposition in post capillary venules in the liver and heart [12,13], suggesting a role of this protein in nanoparticle mediated platelet aggregation.

Silica nanoparticles of different sizes were found to activate glycoprotein IIb/IIIa and to induce the expression of P-selectin [14] in platelets. On the other hand, silica nanoparticles are known to induce oxidative stress in several cell lines including endothelial cells [15] and leucocytes [16,17], a process that in vivo may indirectly induce platelet aggregation.

The interference with the coagulation system is not the only possible mechanism that may induce vascular occlusion. Nanoparticles have a strong tendency to agglomerate in water. The degree and kinetics of agglomeration are controlled by size, shape and surface chemistry of the particles. Strong repulsive electrostatic charges and steric hindrance may stabilize the nanoparticles and prevent agglomeration. In the bloodstream, agglomeration is related to the formation of a biocorona that modifies the electrostatic and steric repulsion among particles [18]. Finally, protein–protein interaction may lead to bridging among particles thus promoting agglomeration [19].

In the present study, a sample set of six silica and carbon nanoparticles with definite size and morphology was used to explore the effect of size and surface properties on the protein corona composition, agglomeration in plasma, platelet aggregation, activation and VWF-mediated adhesion.


## 2. Materials and methods

*2.1 Reagents.*

Sodium polyacrylate, D-(+)-glucose, thionine acetate salt, phosphate buffered saline powder, EDTA, glutathione reduced and 5,5′-dithiobis(2-nitrobenzoic acid), tetraethyl orthosilicate (TEOS) were obtained from Sigma-Aldrich (Germany). 5,5-dimethyl-1-pyrroline-N-oxide(DMPO) was obtained from Cayman chemicals (USA). Ultrapure water was obtained from a Milli Q Plus system (Millipore, Bedford, MA, USA) and was always used freshly prepared. All other chemicals and solvents used

were at least of analytical grade. When not otherwise specified, other reagents were purchased from Sigma-Aldrich.

*2.2 Synthesis of carbon nanoparticles.*

Carbon nanoparticles (CNP) were produced starting from glucose using a one-step hydrothermal process as described in Kokalari et al. 2019 [20]. Briefly, glucose was dissolved in 50 ml of ultrapure water followed by the addition of 15 mg of sodium polyacrilate. The solution was introduced in a pressure reactor system (Büchi AG) and heated at 190°C for 3 or 8 h. Synthesis parameters are described in details in table 1. CNP were then purified using ultrapure water by filtration for large carbon nanoparticles (CNP-L) or tangential flow ultrafiltration (Vivaflow 50R, MW 30 kDa) for the medium and small carbon nanoparticles (CNP-M and CNP-S).

|  | Glucose (g) | Surfactant (mg) | Time (h) | Temperature, (°C) |
|---|---|---|---|---|
| **CNP-S** | 2 | 15 | 3 | 190 |
| **CNP-M** | 2 | 15 | 8 | 190 |
| **CNP-L** | 5 | 15 | 8 | 190 |

**Table 1.** Synthesis parameters used for CNP

*2.2 Synthesis of silica nanoparticles.*

The silica nanoparticles (SNP) were prepared by hydrolysis and condensation of TEOS in the presence of ammonia as a catalyst, based on the Stöber process [21]. Briefly, a defined amount of TEOS was added dropwise, under magnetic stirring, at room temperature, to a solution of ethanol, ammonia (33%) and ultrapure water. The detailed protocols are summarized in table 2.

The suspensions were subjected to repeated centrifugation steps at 11.000 rpm, for 15 min, in ultrapure water and ethanol in order to isolate and wash the nanoparticles. The purified nanoparticles were suspended in ultrapure water and stored at 4°C.

|         | TEOS (ml) | Ethanol (ml) | NH$_3$ (ml) | H$_2$O (ml) | Time (min) |
|---------|-----------|--------------|-------------|-------------|------------|
| SNP-S   | 0.756     | 20           | 0.852       | 0.831       | 40         |
| SNP-M   | 0.756     | 20           | 1.704       | 1.067       | 40         |
| SNP-L   | 0.330     | 44           | 18          | -           | 30         |

**Table 2.** Synthesis parameters for silica nanoparticles

*2.3 Scanning Electron Microscopy (SEM).*

Nanoparticle morphology was characterized using scanning electron microscopy, SEM Zeiss Evo 50XVP (Assing). Carbon and silica nanoparticles suspensions were diluted up to 0.05 mg/ml in ultrapure water. A volume of 20 μl of the diluted suspensions was mounted on aluminium stubs, using double-sided adhesive carbon tape and silicon wafers. Samples were dried overnight at room temperature. In the case of silica nanoparticles, the samples were sputter-coated with thick gold film (~ 17 nm) under argon atmosphere to improve secondary electron emission during SEM imaging. Nanoparticle morphology was observed at an acceleration voltage of 20 kV.

*2.4 Dynamic Light scattering (DLS).*

The mean diameter and polydispersity index (PDI) of nanoparticles were obtained using a Zetasizer (Nano ZS Malvern Instruments, UK) based on the dynamic light scattering (DLS) technique. Measurements were performed on purified nanoparticles by analysing 0.5 ml of suspension in ultrapure water, placed in a square polystyrene cuvette, at 25 °C. PBS 0.01 M, pH 7.4, Sigma Aldrich, was used as a diluent in the case of the evaluation of the size after the protein corona formation.

*2.5 Nanoparticle Tracking Analysis (NTA).*

Analysis of the size distribution and concentration of CNP and SNP were performed by NTA using a Nanosight NS300 (Malvern, UK) equipped with a blue laser (488 nm) and a quartz chamber for sample injection, equipped with an O-ring top plate. For nanoparticles-hard protein corona

complexes, the samples were diluted in PBS, 0.01 M, pH 7.4. Dilution factor was chosen in order to obtain 30 particles per frame, as suggested by the manufacturer's recommendations. The measurement duration was set at 60s.

## 2.6 ζ-potential.

Zeta-potential measurements were performed based on the Electrophoretic Light Scattering (ELS) technique, using Zetasizer (Nano ZS Malvern Instruments, UK) as a function of the pH in the range from 2-9. The nanoparticles suspensions were diluted in ultrapure water at a final concentration of 0.5 mg/ml. The pH of the suspensions was adjusted by adding diluted NaOH or HCl solutions and the samples were introduced in a disposable folded capillary cuvettes (Malvern Panalytical).

## 2.7 Protein corona characterization.

### 2.7.1 Procurement and preparation of plasma.

The human plasma was obtained from healthy donors kindly provided by the Irish Blood Transfusion Service (IBTS), St. James Hospital, Dublin. The plasma from eight different donors was mixed, aliquoted and stored -80°C until use. Before using, the plasma was thawed and centrifuged at 16.000 rpm, 3 min, in order to discard any precipitated protein.

### 2.7.2 Methods.

Carbon and silica nanoparticles were incubated with different concentrations of human plasma diluted in PBS 0.01M, pH 7.4 (Sigma Aldrich) at 37°C under agitation (150 rpm). The number of nanoparticles in all samples was optimized in order to ensure a total surface area of $1.0 \times 10^{-2}$ $m^2$. After the incubation, in order to obtain nanoparticles-hard protein corona complexes, the samples were washed three times by centrifugation as previously described [22]. After the last washing step, the pelleted samples were suspended in PBS, 0.01 M, pH 7.4, and the denaturizing solution, prepared with dithiothreitol and 3x blue loading buffer that contained DTT in a ratio of 1:10 (New England

biolabs) and following the manufacturer instructions. The samples were sonicated for 5 minutes in an ultrasonic bath and then incubated for 5 minutes at 95 °C to complete the protein denaturation. The samples were loaded in a 10-wells 12% stacking gel and the electrophoretic analysis was conducted at 130 V. After the electrophoretic separation, the gels were stained in Imperial Protein stain, (Thermo Scientific) for 1 h and distained overnight (in ultrapure water). The densitometry analysis was performed using the software ImageJ (NIH).

2.7.3 Mass spectrometry analysis

Samples were run on SDS-PAGE for 10 min before the protein bands were excised from the gel. The proteins in the gel pieces were reduced with dithiothreitol, alkylated with iodoacetamide and digested with trypsin (Promega Corporation) overnight at 37°C. The peptides were then extracted from the gel matrix and prepared for MS analysis by using Pierce C18 Tips (Thermo Fisher) following the manufacture procedure.

Peptide samples were analyzed on a quadrupole Orbitrap (Q-Exactive, Thermo Scientific) mass spectrometer equipped with a reversed-phase NanoLC UltiMate 3000 HPLC system (Thermo Scientific). Samples were loaded onto C18 reversed phase columns (10cm length, 75µm inner diameter) and eluted with a linear gradient from 2 to 27% acetonitrile containing 0.5% acetic acid in 58 min at a flow rate of 250nL/min. The injection volume was 5µl. The mass spectrometer was operated in data dependent mode, automatically switching between MS and MS2 acquisition. Survey full scan MS spectra (m/z 300 – 1600) were acquired in the Orbitrap with a resolution of 70,000. MS2 spectra had a resolution of 17,500. The twelve most intense ions were sequentially isolated and fragmented by higher-energy C-trap dissociation.

MS raw files were processed with MaxQuant software (version 1.6.2). The peak lists were searched against the human FASTA database. The search included the modifications of cysteine carbamidomethylation, methionine oxidation and protein N-terminal acetylation. A maximum of two missed trypsin cleavages were allowed in the database search. The false discovery rate for both

peptides and proteins was set at 1%. After that, the ProteinGroup file from Maxquant was processed, filtered and analysed with Perseus software to generate the top abundance table, hierarchical clustering graph and numeric Venn diagrams.

## 2.8 Preparation of blood and PRP.

### 2.8.1 Ethics statement

Blood collection for this study was approved by the Royal College of Surgeons in Ireland and Beaumont Hospital ethics committees. Written informed consent was obtained from all donors prior to phlebotomy. All blood samples were taken in accordance with the declaration of Helsinki.

The blood plasma used for the corona studies was obtained from the Irish Blood Transfusion service (IBTS) St Vincent hospital and the use is covered by the RCSI REC 1246b

### 2.8.2 Study participants

25 healthy donors were recruited for this study. All donors had no previous history of any major disease and were free from any medication such as statins, antihypertensive medication, antiplatelet agents such as aspirin, or anti-inflammatory medications such ibuprofen, for at least 12 days prior to blood draw.

### 2.8.3 Preparation of blood and PRP

Venous blood was drawn from the antecubital vein using a 19-gauge butterfly needle connected to a sterile polypropylene syringe. Blood was drawn into 3.2% (w/v) trisodium citrate anticoagulant (1:9 volume of citrate to blood, final citrate concentration of 0.32%). Blood samples were kept at room temperature with gentle rocking and used within 1 hour of phlebotomy. Whole blood cell counts were recorded for each donor, using a Sysmex-KX21N haematology analyser (Kobe, Japan). Blood samples were centrifuged at 170 g for 10 min to obtain platelet-rich plasma (PRP) (Centrifuge 5417R, BIOTOOLS, CA).

*2.9 Light Transmission Aggregometry (LTA).*

Platelet aggregation was monitored by light transmission aggregometry (LTA) in a Chronolog-490D aggregometer (CHRONO- LOG® Corporation, Havertown, PA). Adenosine diphosphate ADP and collagen were used as activators of platelet aggregation.

The nanoparticles suspended in phosphate buffered saline (PBS) were added to 250 µl PRP and incubated for 1 minute. The concentration of nanoparticles was calculated on the base of mean diameter and nanoparticles concentration in number (NTA) to have a total of $8.6 \times 10^{-4}$ $m^2$/ml of exposed surface area, equal to 1 mg/ml for CNP-S. In the case of CNP-L the concentration was lower to avoid interference ($7.25 \times 10^{-5}$ $m^2$/ml). 2.5 µl of 10 µM ADP or 12.5 µl of 10 µM collagen was then added and aggregation monitored for 5 minutes with the suspension continuously stirred. Optical density was also measured for nanoparticles suspended in PRP in the absence of agonists for up to 40 minutes of incubation. PRP without nanoparticles was used as control. The data are expressed as mean of three independent experiments.

*2.10 Flow Cytometry Fluorescence activated cell sorting (FACS).*

Flow cytometry fluorescence-activated cell sorting (FACS) was used to evaluate platelet activation. Nanoparticles were suspended in PRP at the same concentration used for LTA. 2.5 µl of the fluorophore-conjugated antibody (CD62P) (1.5 µg/ml) (Becton Dickinson, Oxford, UK), which binds P-Selectin and 87.5 µl of PBS were added to 10 µl of the suspension and incubated for 10 minutes. Reactions were stopped by the addition of PBS to a final volume of 1ml. Mean fluorescent intensity (MFI) was read on a Beckman Coulter Cytomics FC500 flow cytometer. The experiments were repeated by adding 5 µl of ADP (10µM). The data are expressed as mean of three independent experiments.

*2.11 Dynamic Platelet Function Assay (DPFA).*

The DPFA is a well-characterised real-time assay of platelet interaction with von Willebrand Factor (VWF) under conditions of arterial shear [23-25].

The initial phases of platelet aggregation were assayed using the DPFA as previously described [23-24]. Briefly, custom parallel plate perfusion chambers were coated overnight with 100 µg/ml VWF, washed with phosphate-buffered saline and blocked with 1% bovine serum albumin for 1 hour prior to use. Whole blood was labelled with 1µM $DiOC_6$ (Sigma Aldrich, Ireland) for 5 minutes at 37 ℃ prior to perfusion through the chamber at an arterial rate of shear ($1500\ s^{-1}$). Platelet translocation behaviour was recorded using real-time video microscopy at a rate of 19 frames per second. Image stacks were analysed by a custom-designed and validated software package [23]. The assay measurements obtained from this analysis include the number of platelets that interacted with the VWF surface (Platelet tracks), the number of platelets that translocate over VWF (Translocating platelets), the average speed at which platelet translocation occurred (Platelet translocation speed), the distance a platelet translocated along the VWF surface (Platelet translocation distance), the number of platelets that stably adhered to the VWF-coated surface (Static platelets), and the percent surface coverage on the final frame (Percentage of platelet surface coverage). For this study we just looked at the platelet adhesion parameters.

## 3.     Results

*3.1 Preparation of the libraries of silica and carbon nanoparticles.*

In this study we synthetized two matching set of nanoparticles of silica and carbon that had similar mean hydrodynamic diameters. DLS and NTA mean hydrodynamic diameters (table 3) confirmed a similar size distribution across the two materials.  The low polydispersity indexes indicate high colloidal stability and narrow size range distribution.

| | DLS | | | NTA | |
|---|---|---|---|---|---|
| | **Hydrodynamic diameters (nm)** | **Standard Dev.** | **PDI** | **Hydrodynamic diameters (nm)** | **Standard Dev.** |
| **SNP-S** | 114.1 | ±0.351 | 0.081 | 115.0 | ±1.52 |
| **SNP-M** | 235.1 | ±4.754 | 0.012 | 217.3 | ±4.16 |
| **SNP-L** | 488.1 | ±5.387 | 0.031 | 333.3 | ±14.5 |
| **CNP-S** | 179.5 | ±3.482 | 0.074 | 128.3 | ±2.52 |
| **CNP-M** | 259.7 | ±2.193 | 0.010 | 232.0 | ±6.08 |
| **CNP-L** | 485.2 | ±2.452 | 0.123 | 349.0 | ±4.36 |

**Table 3.** Mean of hydrodynamic diameters, PDI and standard deviation of each sample measured after purification obtained with DLS (white background), compared with the mean of hydrodynamic diameters and standard deviation obtained using NTA (grey background).

The hydrodynamic diameters measured by NTA were similar to those measured by DLS, except for the large samples, for which the NTA value was lower. In fact, NTA, but not DLS, detected four populations of particles having a different size (SI) that, in DLS contribute to the mean diameter observed. This is in agreement with the PDI higher than the others.

In figure 1 the representative SEM images of the samples are presented. All particles appear perfectly spherical with a uniform size, the latter confirming the DLS analysis.
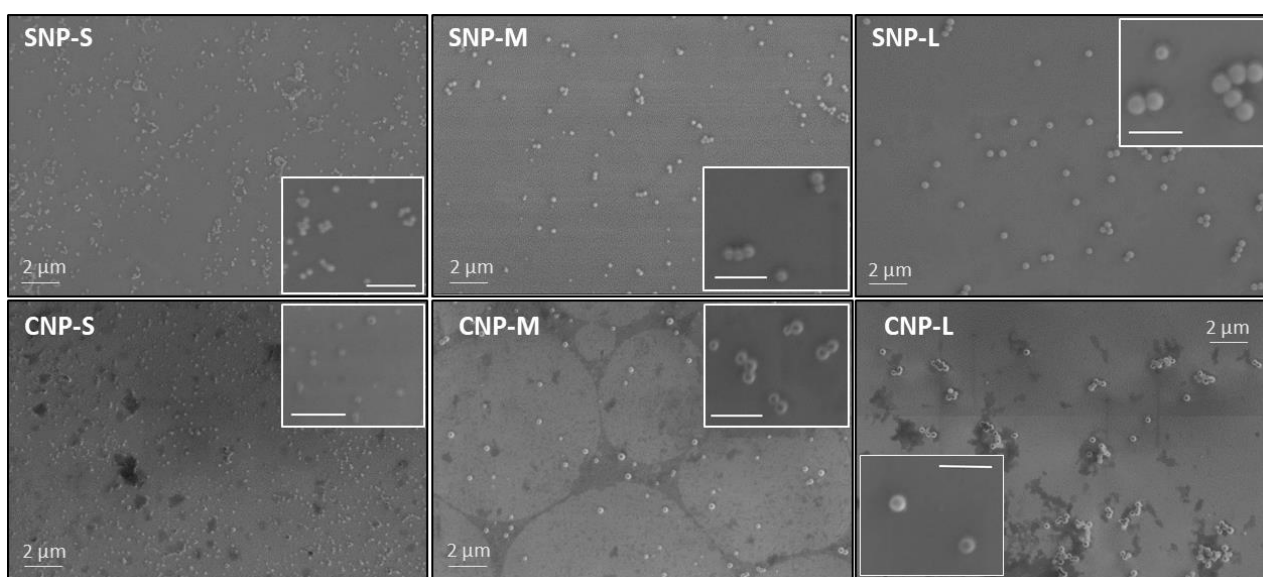


**Figure 1.** SEM micrograph of silica and carbon nanoparticles

The $\zeta$- potential of the samples was measured by ELS in the pH range from 2 to 9 (figure 2a)
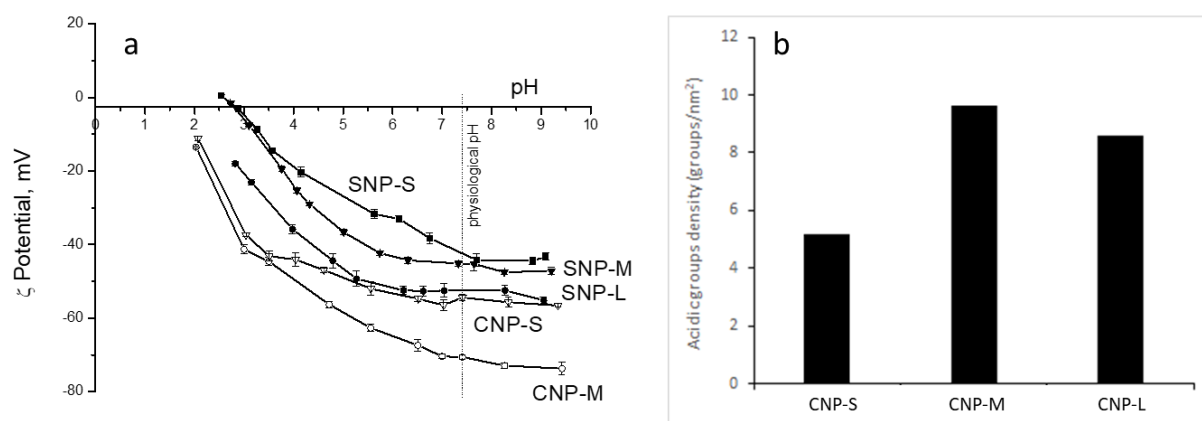


**Figure 2.** a) Zeta potential versus pH curves for carbon nanoparticles (CNP-M and CNP-S) and silica nanoparticles (SNP-L, SNP-M and SNP-S) suspended in water. b) Density of acid groups exposed at the surface of carbon nanoparticles.

As expected, both silica and carbon samples exhibited a negative zeta potential across the whole pH range. It gradually increased with increasing of the pH of the suspension never reaching positive values indicating the presence at the surface of weakly acidic groups. In the case of carbon nanoparticles, acidic carboxylic or phenolic groups formed during the synthesis are expected, while silica exposes at the surface hydroxyl groups. At physiological pH (7.4) all particles exhibit a high $\zeta$- potential in the range of -40/-70 mV. Carbon nanoparticles exhibit a $\zeta$- potential more negative than the correspondent silica nanoparticles. Note that the $\zeta$- potential curve of CNP-L is not reported since this samples rapidly agglomerate by lowering the pH value, making unfeasible the measurement.

The presence of acidic groups at the surface of carbon nanoparticles was quantified by titration using the dye thionine acetate [26]. In Figure 2b the density of acidic groups for carbon nanoparticles is reported. The three samples differ slightly in terms of the density of acidic surface groups, with the

small NPs having the lowest density, in agreement with the observed less negative ζ- potential value. The density of the acidic groups for silica was not determined since widely reported in literature [27, 28].

*3.2 Physico chemical and proteomics characterisation of the NP-Hard corona*

We then evaluated how the NP physico chemical properties would affect the biomolecular corona formation. For this purpose, we exposed the same surface area of three-sized NP of silica and carbon to increasing concentrations of human plasma, 10% to 80%, to mimic the *in vitro / in vivo* conditions respectively. After 1 hour incubation at 37°C, the NP-corona complexes were separated from unbound proteins and washed three times by centrifugation. SDS-PAGE and MS were used to obtain information on the biomolecular corona composition in each sample. In figure 3 the SDS-PAGE gels for the small silica and carbon nanoparticles are shown. The corona composition between the two materials has some similarities when incubated at 10% of plasma, however it became highly specific to the NP surface properties at higher concentration as we detected a significantly difference in the corona composition.
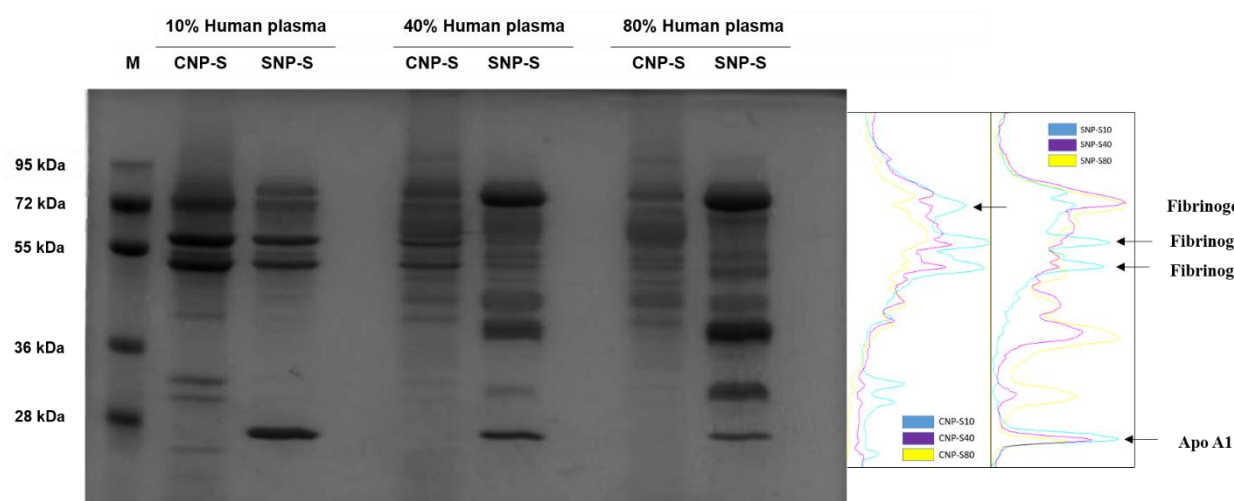


**Figure 3.** SDS-PAGE gel of hard protein corona formed after 1h of incubation in human plasma. The gel bands correspondent to fibrinogen and apolipoprotein A1 are shown.

In particular, at 10% of plasma, both NPs preferentially adsorb three gel bands of 72, 60 and 50kDa, later identified as fibrinogen alpha, beta and gamma chain respectively, but significant differences

were also observed at lower molecular weight where a gel band of 25kDa was detected in the silica corona while in the carbon NP corona was formed by 3 gel bands in the region of 36-30kDa and a less pronounced band of a MW lower than 28kDa. At higher plasma concentration, the corona composition of the SNP changed significantly where the fibrinogen gel bands were displaced by three predominant bands of 90kDa and a duplet of 50kDa, later identified with histidine rich glycoprotein. These findings were in agreement with a previous study where a similar effect was detected for 200nm silica NP as previously reported [22]. Notably, the bands of correspondent to fibrinogen become more attenuated at higher percentage of plasma in silica, but remain abundant in carbon corona (figure 4). Small molecular weight bands also became displaced at higher plasma concentration.

Little differences in the protein corona composition were found depending upon the size of the nanoparticles (SI) suggesting that the surface curvature, in the range considered, plays a minor role.
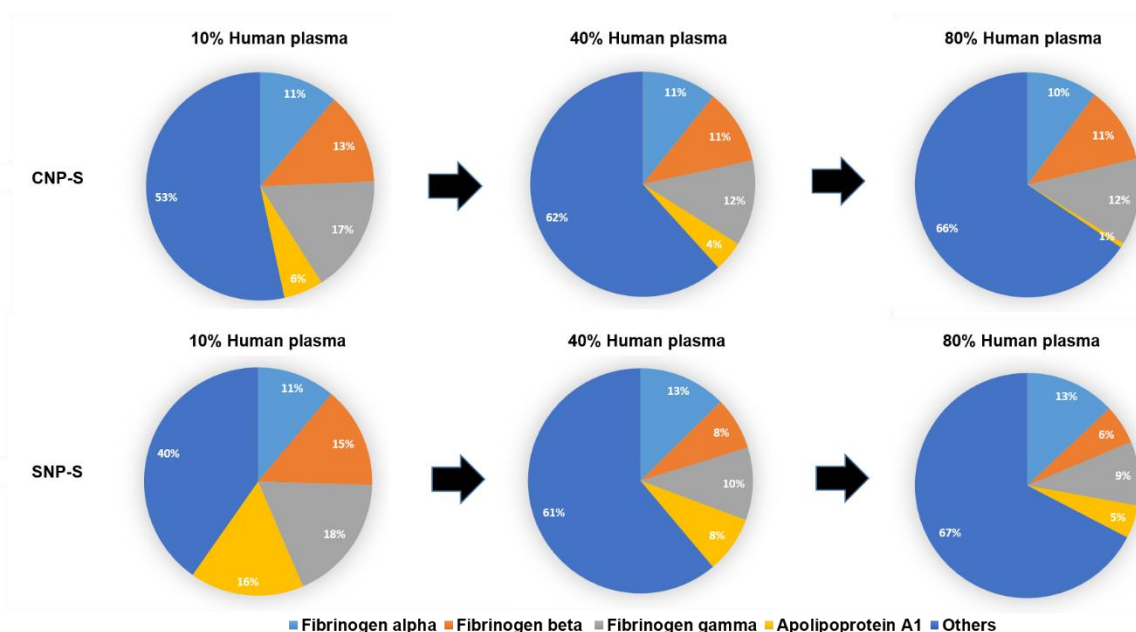


**Figure 4**. Abundance of fibrinogen and apolipoprotein A1 in silica and carbon corona at different plasma concentration.

Label-free mass spectrometry was used to obtain the semi quantitative protein abundance of the corona of small silica and carbon NP across three different plasma concentrations. A total of 118 proteins were found in the biomolecular corona of small carbon and silica NPs after incubation with

human plasma 10, 40 and 80%. Table 4 contains the top 20 proteins detected in each condition by MS.

| Order of abundance | SNP-S | | | CNP-S | | |
|---|---|---|---|---|---|---|
| | 10% Human plasma | 40% Human plasma | 80% Human plasma | 10% Human plasma | 40% Human plasma | 80% Human plasma |
| 1 | Fibrinogen gamma chain | Kininogen-1 | Kininogen-1 | Fibrinogen beta chain | Fibrinogen beta chain | Kininogen-1 |
| 2 | Fibrinogen alpha chain | Fibrinogen alpha chain | Histidine-rich glycoprotein | Fibrinogen alpha chain | Fibrinogen gamma chain | Fibrinogen alpha chain |
| 3 | Fibrinogen beta chain | Fibrinogen beta chain | Kallikrein B | Fibrinogen gamma chain | Fibrinogen alpha chain | ITIH4 protein |
| 4 | Apolipoprotein A-I | Fibrinogen gamma chain | Coagulation factor XI | Apolipoprotein B-100 | Kininogen-1 | Fibrinogen beta chain |
| 5 | Kininogen-1 | Apolipoprotein A-I | Plasminogen | Histidine-rich glycoprotein | ITIH4 protein | Fibrinogen gamma chain |
| 6 | Apolipoprotein E | Histidine-rich glycoprotein | Apolipoprotein A-I | Kininogen-1 | Vitronectin | Coagulation factor XI |
| 7 | Histidine-rich glycoprotein | Kallikrein B | Plasma protease C1 inhibitor | Vitronectin | Apolipoprotein B-100 | Vitronectin |
| 8 | Apolipoprotein B-100 | Coagulation factor XI | Fibrinogen alpha chain | Complement C1q | Plasma kallikrein | Kallikrein B |
| 9 | Kallikrein B | Apolipoprotein E | Apolipoprotein B-100 | Complement component 4B | Apolipoprotein E | Histidine-rich glycoprotein |
| 10 | Plasma protease C1 inhibitor | Coagulation factor XII | Fibrinogen beta chain | Complement factor H | Complement component 4B | Apolipoprotein B-100 |
| 11 | Selenoprotein P | Selenoprotein P | Fibrinogen gamma chain | Apolipoprotein E | Coagulation factor XI | Apolipoprotein E |
| 12 | Coagulation factor XII | Plasminogen | Serum albumin | ITIH4 protein | Serum albumin | Serum albumin |
| 13 | ITIH4 protein | Plasma protease C1 inhibitor | ITIH4 protein | Serum albumin | Complement factor H | Complement C3 |
| 14 | Serum albumin | Serum albumin | Selenoprotein P | Complement component 1 | Complement component 1 | Ig gamma-3 chain C region |
| 15 | Complement C3 | ITIH4 protein | Apolipoprotein E | Complement C3 | Complement C3 | Isoform C of Proteoglycan 4 |
| 16 | Plasminogen | Ig gamma-3 chain C region | serine protease inhibitor | Kallikrein B | serine protease inhibitor | Ig mu chain C region |
| 17 | Coagulation factor XI | Complement C3 | Ig kappa chain C region | Apolipoprotein A-I | Complement factor H-related protein 1 | Selenoprotein P |
| 18 | Isoform C of Fibulin-1 | Ig alpha-1 chain C region | Ig gamma-3 chain C region | Ig gamma-3 chain C region | protease C1 inhibitor | serine protease inhibitor |
| 19 | Apolipoprotein A-II | Apolipoprotein A-II | Ig alpha-1 chain C region | Ig mu chain C region | Complement C1q | Ig kappa chain C region |
| 20 | Apolipoprotein C-I | Vitronectin | Complement C3 | Coagulation factor XI | Ig gamma-3 chain C region | Complement factor H-related protein 1 |

**Table 4:** Top 20 most abundant proteins in small silica (SNP-S) and carbon (CNP-S) hard corona samples at three different plasma concentration (10, 40, 80%) based on the LFQ intensity.
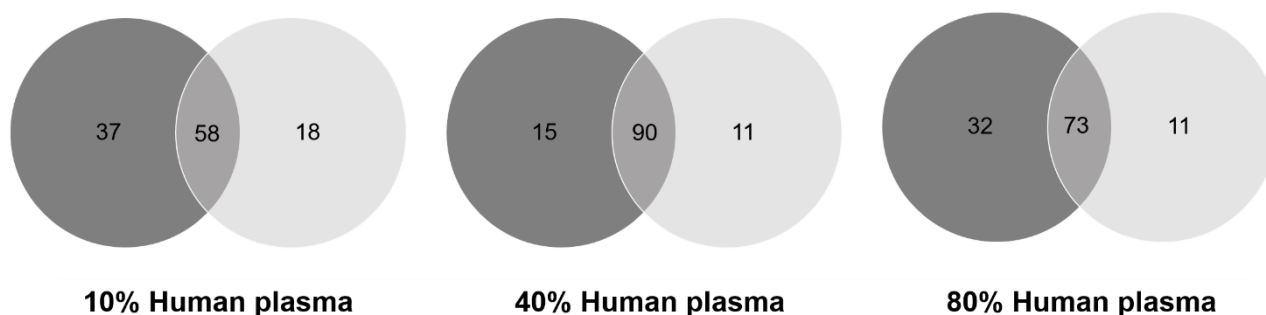
**Figure 5:** Venn diagrams showing the number of proteins shared by small silica (Black) and carbon NP (Grey) protein corona formed at different plasma concentrations.

Venn diagrams (figure 5) highlighted that the majority of the proteins were detected both in the SNP and CNP at the higher plasma concentrations, while a minor overlap occurred at 10%. However, a pronounced difference was observed when we compared the protein abundance by means of the label free quantification (LFQ) across all conditions (table 4 and figure 6).

The presence of fibrinogen decreased firmly with increasing plasma concentration (80%) in silica nano-corona, and was displaced by less abundant but with higher affinity proteins, like histidine rich glycoprotein, kallikrein B and plasminogen confirming the SDS-PAGE findings and the literature.

Apolipoprotein A1, a major protein that form the HDL, has shown to have a preferential affinity towards silica NP where it was detected across all conditions. The findings were also in agreement with the SDS-PAGE where a gel band of 28kDa was detected only for silica NP. Other HDL apolipopoproteins including apoA2 and A4 are also more abundant in silica corona than carbon one, which might be attributed to the surface chemistry.

Interestingly, fibrinogen was strongly bound to the CNP also at higher concentration of plasma, although with a less amount. Similarly, ApoB100, ApoB100, a protein that forms the VLDL/LDL, and histidine rich glycoprotein were enriched at 10% of plasma but they become displaced by other proteins, such as vitronectin and ITIH4 at higher concentration of plasma in CNP. Interestingly,

albumin (66 kDa), the most abundant protein in human plasma, is outside the top 10 proteins identified with MS in all samples confirming that the composition of the protein corona, is independent to the protein original abundance.
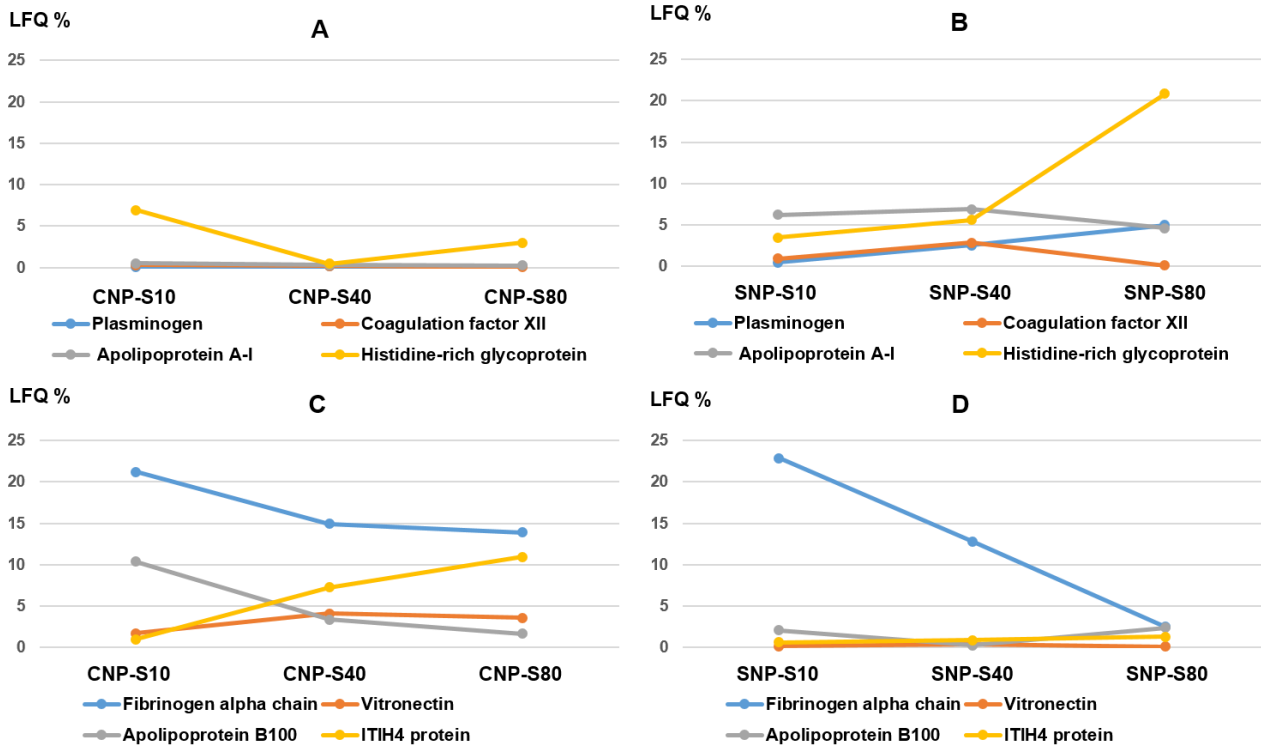


**Figure 6:** Relative concentration of relevant proteins on small silica (SNP) and carbon (CNP) coronas at plasma concentrations of 10, 40 and 80%. The percentages were calculated based on the total LFQ intensity in each sample.

Protein grouping (Figure 7) confirmed that the coagulation factors are highly enriched in the corona across all conditions although with different percentage (55-75%)
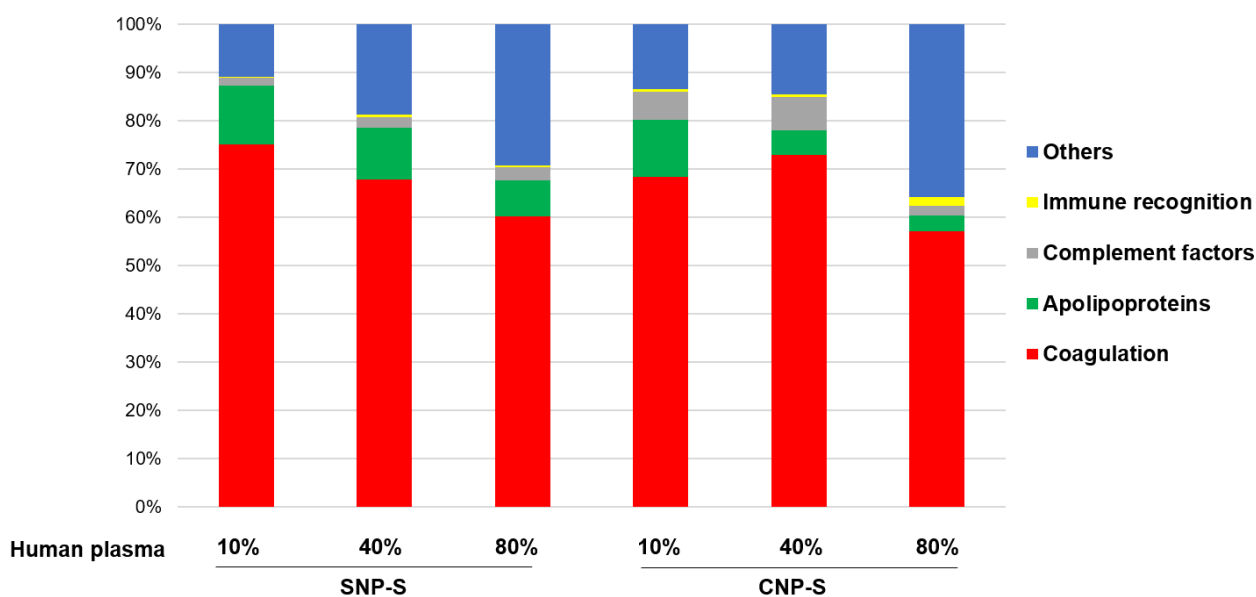
**Figure 7:** Classification of the human plasma corona proteins identified on small silica (SNP-S) and carbon (CNP-S) NPs according to their biological functions. The LFQ intensity is used to calculate the percentages of protein groups.

In terms of molecular weights, most proteins found in the corona of both nanomaterials are between 20-60 kDa in weight, which accounts for about 70% of proteins (SI). Around 8% of the total corona proteins have high molecular weights (>150 kDa).

### 3.3 Effect of hard corona on agglomeration

The effect of the protein corona on the tendency of nanoparticles to agglomerate was evaluated by preparing the protein corona using the protocol described above, re-suspending the particles in PBS and measuring the size distribution by NTA. The mean hydrodynamic diameters of the particles with the protein corona generated at three different plasma concentrations (10, 40 and 80%) are compared in Figure 8 with the hydrodynamic diameter of the pristine nanoparticles.
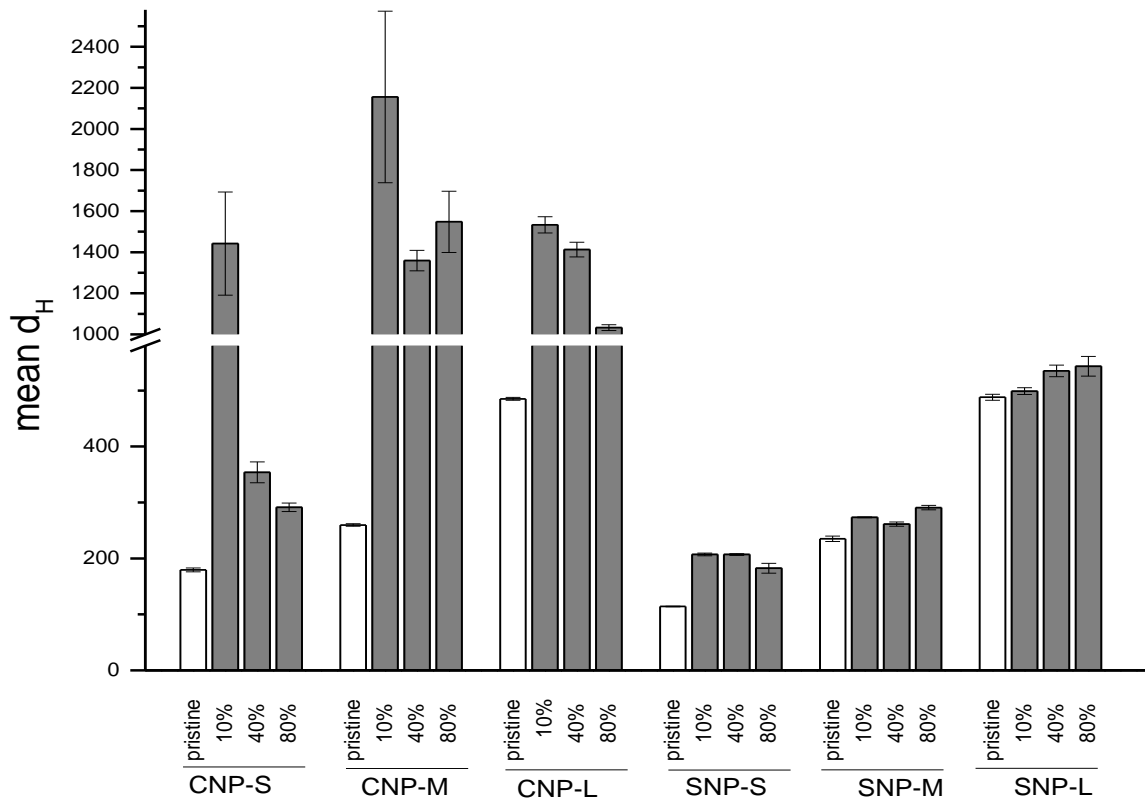
**Figure 8.** Effect of hard corona formed at different plasma concentrations on nanoparticles agglomeration in water.

The presence of the hard protein corona induced a substantial agglomeration in all carbon nanoparticles. This effect was evident for the protein corona formed in plasma at 10% concentration. By increasing the plasma concentration, the mean hydrodynamic size of the small carbon nanoparticles becomes similar to the nanoparticles without the protein corona. Conversely, large and mean size carbon nanoparticles remain highly agglomerated with a mean size higher than 1 µm. In the case of silica nanoparticles no agglomeration was observed at all concentrations of plasma tested.

*3.4 Platelet aggregation*

The effect of the nanoparticles on platelet aggregation was measured using light transmission aggregometry (LTA). NPs were added to platelet rich plasma (PRP) in the absence or presence of two platelet activators, collagen and ADP.

In figure 9a,b the percent aggregation of platelets in after 5 minutes from the addition of ADP or collagen induced by silica and carbon samples is reported. When platelets were activated by collagen, a slight but significant increase in aggregation was observed for all samples. A similar trend was also observed in the presence of ADP as activator, albeit the values did not significantly differ from the control. In the case of medium and large CNP, a progressive decrease in optical density was observed upon the addition of the nanoparticles (SI). To monitor this process, the optical density was measured up to 40 minutes after addition of the nanoparticles in the absence of the activators (Figure 9c, SI). Significant aggregation was detected for both silica and carbon medium and large nanoparticles, with a major effect observed for CNP-L. This effect was previously reported by Bihiari and co-workers [9] for SWCNTs and was attributed to the formation of nanoparticle-platelet aggregates. Note that for large and medium size carbon nanoparticles, black aggregates were clearly visible at the end of the experiments (SI).
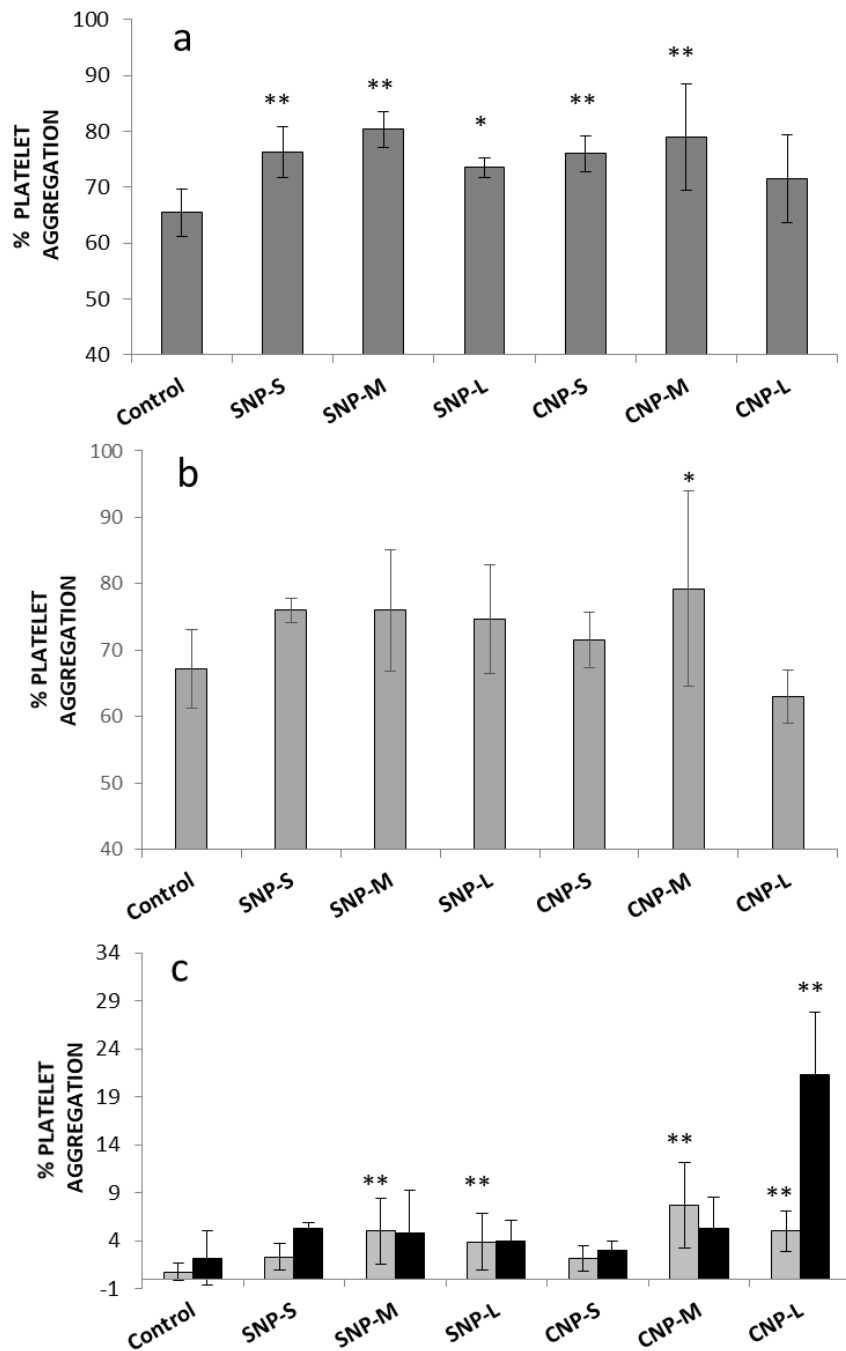
**Figure 9:** Effect of nanoparticles on platelets aggregation. A) platelets activated with collagen; b) platelets activated with ADP; c) platelets not activated after 5 (grey bars) and 40 (dark bars) minutes of incubation. ** $p < 0{,}01$ , * $p < 0{,}05$.

## 3.5 Platelet activation

The activation of platelets by the silica and carbon samples was evaluated by flow cytometry.

Activation was evaluated by using a specific antibody, which binds the antigen CD62P (P-Selectin)

present on the surface of activated platelets (Figure 10). No significant activation was detected in the absence of activators. When platelets were activated with ADP, an increase of activation was observed for both silica and carbon nanoparticles of mean size only. This increase was evident, but not statistically significant due to the high variability of the response form one donor to the other. The intensity of forward (FS) and side (SS) scattered light were also measured to evaluate the size of platelets and the granularity respectively. A slight increase of platelet size was observed in the presence of the silica and carbon NPs of medium size. The analysis of the platelet activation by flow cytometry is particularly critical in the presence of particles due to the possible interference in the intensity of scattered light. However, here this is not the case, since particles are clearly visible in the SC-FC plot (SI) as separate population having a size smaller than platelets, and therefore excluded by the measurement. However, possible interference may derive form aggregates.
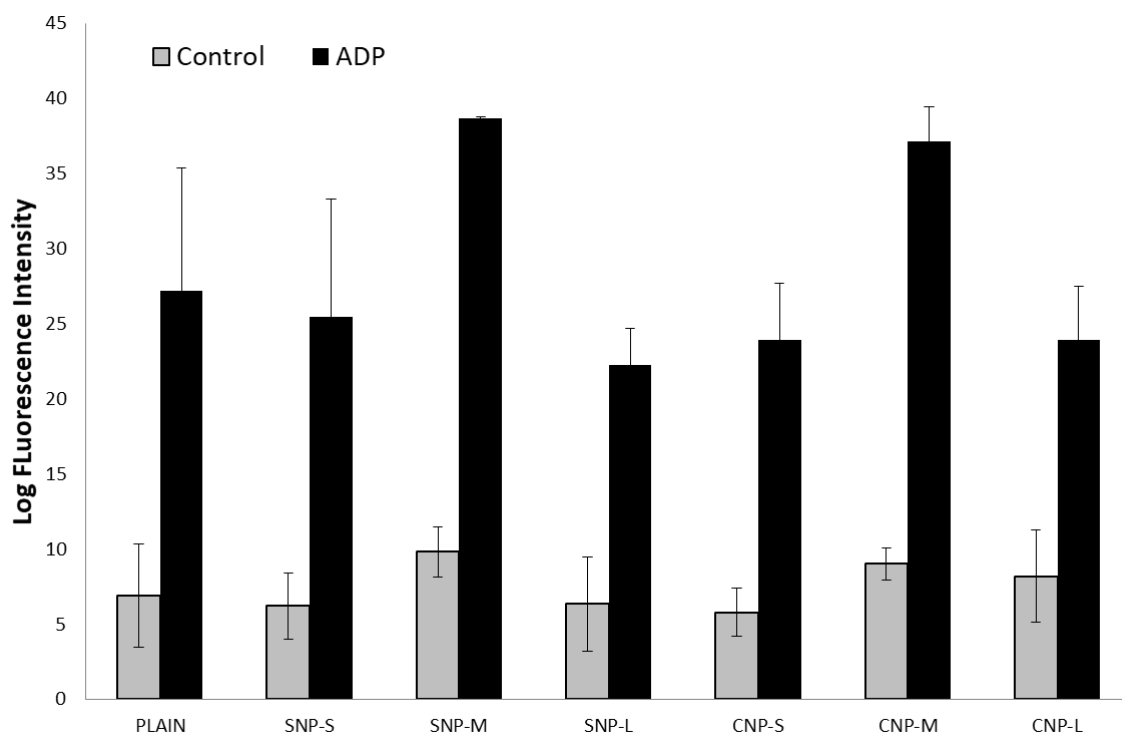


**Figure 10.** Effect of the nanoparticles on platelet activation measured as secretion of P-Selectin

## 3.6    Platelet adhesion

Activated platelets are programmed to adhere to the endothelial wall of damaged blood vessels. Von Willebrand factor protein (VWF) anchored to damaged endothelial cells plays a major role in this process, encouraging platelets to tether, roll and finally adhere at the site of damage. To investigate the possible interference of the nanoparticles on this process the Dynamic Platelet Function Assay (DPFA) was used. This well-characterised assay monitors shear-mediated dynamic platelet interactions with surface-immobilized VWF. Adhesion was measured as total number of platelets adhering to the substrate (figure 11) in the presence or absence of the nanoparticles.
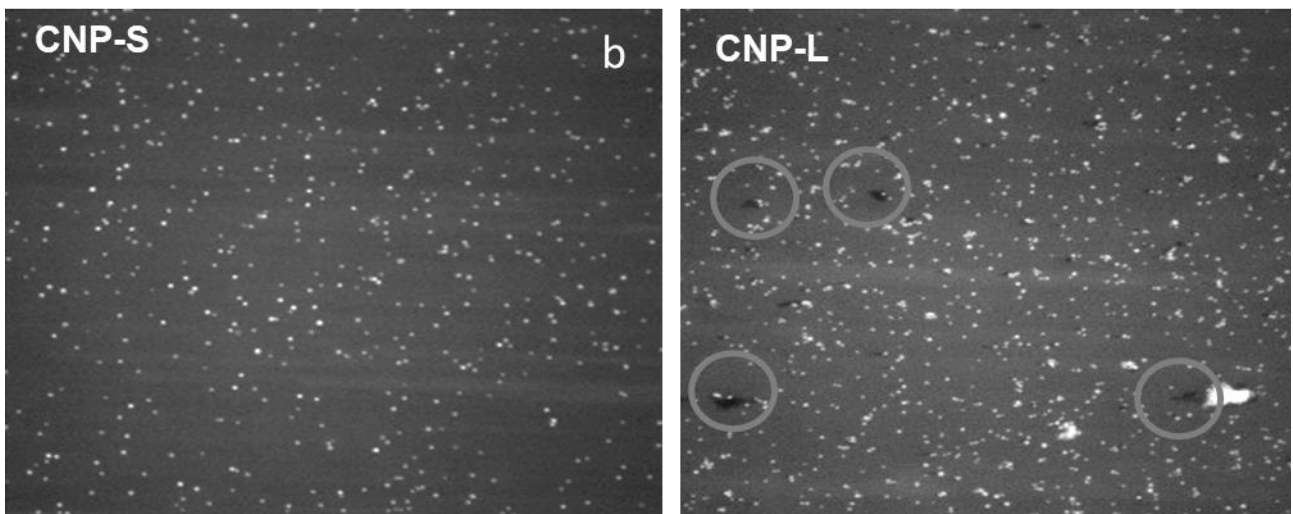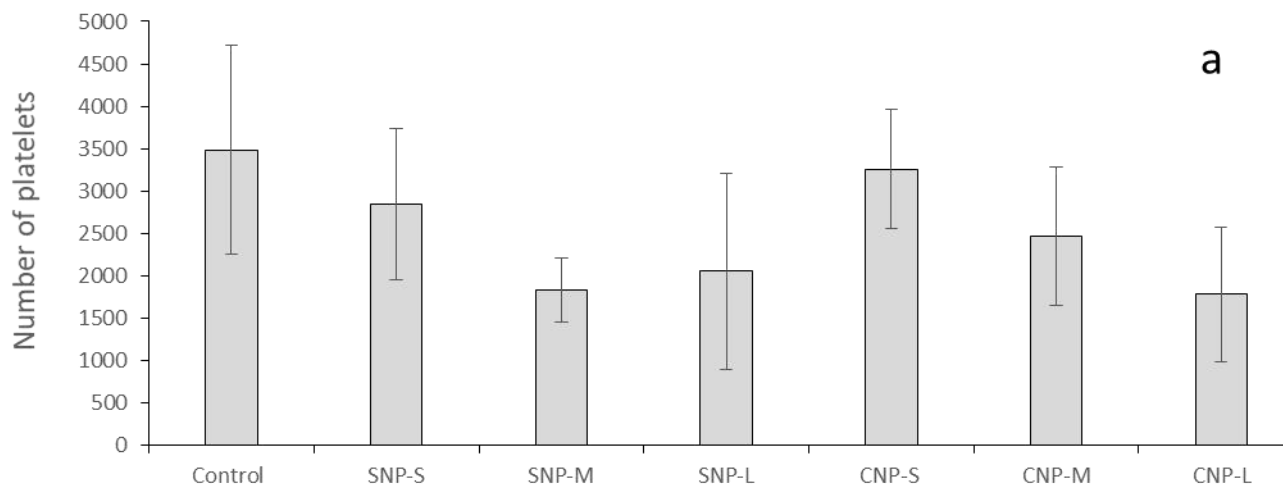
**Figure 11.** Effect of the nanoparticles on platelets adhesion. a) total number of platelets adhering to the substrate; b) and c) representative images of the substrate during the measurements.

A size dependent decrease in the number of platelets adhering to the substrate was detected (Figure 11a). Figure 11b shows two representative images of the VWF coated microfluidic channel captured during the flow run. For CNP-L, large aggregates were observed at the surface of the substrate (circles). These aggregates were not visible for the other samples.

## 4.    Discussion.

The identification of the correlations existing among physical and chemical properties and biological effects is a laborious but necessary process allowing the design of more efficacious and safe substances for medical applications. In the case of (nano)biomaterials this process is more challenging than for molecular substances, due to the higher number of parameters to be controlled. A library of nanomaterials that differ by one single property at time and accurate testing strategies are necessary. This is not always straightforward due to the interdependence between the various chemical and physical properties.

In the present study, two sets of nanoparticles were prepared with the aim to specifically investigate the effect of the surface curvature and surface chemistry on platelet-dependent and independent aggregation, platelet activation and adhesion. Silica and carbon nanoparticles were chosen since both are highly studied for medical applications. Furthermore, being produced by wet methods, the selected  nanoparticles have both hydrophilic surfaces and are negatively charged. Their comparison, therefore excludes surface charge and hydrophilicity as variables to be investigated.  In figure 12 the strategy used to unravel possible SARs is reported.
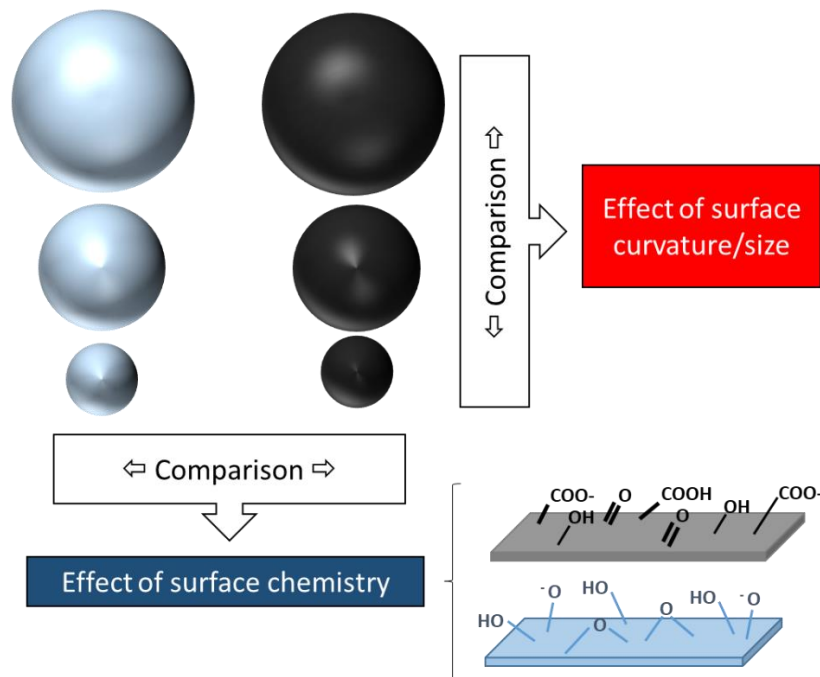
**Figure 12.** Strategy used to unravel possible structure-activity relationships.

This strategy allowed us to identify surface chemistry as key factor in the protein corona composition while both surface chemistry and size modulate a platelet-independent aggregation potential of particles in blood.

Platelet aggregation is a complex process modulated by several chemical and physical parameters. Ordinarily platelets circulate in blood in a quiescent state near the endothelial cells lining the blood vessels without forming stable adhesions. After infringement of the vasculature proteins like von Willebrand factor (VWF), collagen and fibronectin are exposed on the sub endothelial matrix and act as ligands for platelet surface receptors, glycoproteins like GPVI and GPIbα [29-31]. These receptor-ligand interactions initiate a cascade of intracellular responses resulting in amplification of platelet activation through the secretion of soluble agonists including thromboxane A2 (TXA2) and ADP. TXA2 and ADP act jointly with the engaged platelet receptors to mobilize intracellular $Ca^{2+}$, which instigates platelet shape change, degranulation, and up-regulation of the adhesive function of another platelet surface receptor, integrin αIIbβ3 [29]. The active conformation of αIIbβ3 integrin can then bind fibrinogen (FG), VWF and fibronectin with high affinity allowing haemostatic platelets to

aggregate and thrombus formation [32]. FG plays a key role in platelet aggregation, forming bridges between platelets and acting as an aggregation glue. On the other hand, FG also has a key role in surface-driven aggregation.  FG has a high affinity for surfaces [33], and it is commonly present in the protein layer/corona of several materials [22] [34]. On hydrophilic surfaces, this protein tends to be displaced by other proteins by a mechanism known as Vroman's effect [33]. However, in some cases adsorbed FG undergoes conformational changes thus exposing cryptic domains. Platelets may adhere to fibrinogen immobilized onto biomaterials through integrins, a mechanism that may lead to thrombotic events. Furthermore, in the case of NMs, this protein may act as glue in a similar way to that observed with platelets [17], inducing nanoparticle aggregation. However, in this case the effect is not due to the interaction with integrin, but it is a non-specific process due to the tendency of FG to form fibrils similar to fibrin. This tendency is a consequence of specific arrangement of the FG molecule onto surfaces, modulated by the surface properties [19].

Starting from the hypothesis of a possible effect of FG on nanoparticles platelet-dependent or independent aggregation, we firstly investigate whether FG was present on the hard protein corona of the NPs.

Fibrinogen was found in the hard protein corona of both silica and carbon nanoparticles regardless their size, albeit it was relatively more abundant in the protein corona of carbon nanoparticles at high serum concentration when compared with silica. In fact, the amount of FG decreases by increasing the concentration of plasma due to the displacement of FG by proteins having higher affinity for the surface, an effect more evident for silica nanoparticles and already described by some of us elsewhere [22].

Unexpectedly, the presence of the protein corona clearly induces agglomeration of carbon nanoparticles but not of silica. Notably, aggregation was observed for medium CNP and large CNP at all plasma concentrations tested, while in the case of small CNP aggregation was observed only with 10% of plasma, correspondent to the condition used in *in vitro* tests, but not *in vivo*.

The differences observed among silica and carbon nanoparticles might be a consequence of the different composition of the protein corona, or to a different arrangement of protein molecules at the surface, as a consequence of a different ability of the surfaces to interact with the proteins [18]. The affinity of a protein for a certain surface and the mode of interaction rise form the interplay of electrostatic interactions, hydrogen bonding, and hydrophobic forces [28]. Silica and carbon nanoparticles are both negative at physiological pH. However, silica nanoparticles exhibit a less negative $\zeta$- potential when compared with carbon nanoparticles of similar size, likely due to a lower mean Brönsted acidity of the surface, being the density of acidic carboxyl/ phenolic groups at the carbon surface similar to the expected density of silanols (Si-OH) at a fully hydroxylated surface, i.e. of 4-5 groups/nm$^2$ [27-28]. Both surfaces exhibit surface sites able to form hydrogen bonds or hydrophobic interaction with proteins. However, such tendency may be different since hydrogen bonds formation obeys to geometrical constraints due to the directional character of this bond. On the other hand, both silica and carbon surfaces exhibit hydrophobic patches, i.e. siloxane bridges and carbon-carbon bonds respectively. These moieties have a different nature having the first a higher dipolar character.

Previous studies reported fibrinogen-induced aggregation for silica nanoparticles [19,34]. However, in these studies pyrogenic silica samples were used. These materials are very different to silica produced by sol-gel methods, being formed by large aggregates and having a surface with a lower degree of hydrophilicity [16]. A different arrangement of the fibrinogen molecule at the surface of silica is therefore likely. In fact, we previously reported that the tendency of fibrinogen to self-assemble to form fibrin-like fibrils increased by decreasing the hydrophilic character of silica [19].

When incubated in the presence of platelets, silica nanoparticles and small carbon nanoparticles induce only mild aggregation (figure 9), in agreement with what previously found on silica nanoparticles [14]. Aggregation was observed for prolonged time of incubation with large carbon nanoparticles only. This process does not involve platelet activation and appears related to the ability of particles to act as bridges among platelets, similarly to that observed by other authors with other

carbon nanomaterials [9,11]. This was confirmed for large nanoparticles (figure 10), while for medium size particles platelet activation cannot be excluded.

In light of these evidences, the observed reduction of VWF-mediated adhesion of platelets to endothelial wall induced by all NPs should be regarded as a consequence of the sequestration of platelets by particles. In fact, this effect is more evident for large particles.

The different aggregation potential of CNP depending upon their size may explain the contrasting data found in literature on isometric carbon nanoparticles. In fact, secretion of P-Selectin *in vitro* was observed for carbon black [11] but not diesel exhaust particles [9], while platelet aggregation was observed for amorphous carbon nanoparticles but not for the small-sized fullerenes [8]. Note however that limited information relating to the physico-chemical properties of these materials was given by these studies making it difficult to form a critical analysis of the results. Note moreover that while CNT was reported to induce platelet aggregation [8,9] CNP did not. This supports the hypothesis by De Paoli Lacerda and co-workers that an elongated shape is necessary for this process [10].


**Conclusions**

In conclusion, the present study suggest that NP-NP and NP-platelet aggregates may be generated in blood following administration of nanoparticles that are stable and monodisperse in water also without platelets activation. This process should be regarded as concern, since aggregates might induce vessels occlusion in vivo. CNP have an aggregation potential higher than silica nanoparticles. However, the reduction of size to less than 100 nm appears to improve the stability these materials and, possibly, their biocompatibility. Further investigations will be necessary to confirm in vivo this hypothesis.


**Supporting Information**

Supporting Information File 1:

File Name: SI.pdf

File Format: PDF

**Acknowledgements**

# References

1.  Coty, J. B.; Vauthier C. *J. Control. Release* **2018**, 275, 254–268.

2.  Khorasani A. A.; Weaver J. L.; Salvador-Morales C. *Intern. J. Nanomed.* **2014**, 9, 5729–5751.

3.  Fadeel B. *J. Internal Med.* **2013**, 274 (6), 578-580.

4.  Ilinskaya A. N.; Dobrovolskaia M. A. *Nanomedicine* **2013**, 8(5), 773-784. doi: 10.2217/NNM.13.48

5.  Ilinskaya A. N.; Dobrovolskaia M. A. *Nanomedicine* **2013**, 8(6), 969-81 doi: 10.2217/nnm.13.49

6.  Dobrovolskaia M. A.; Patri A. K., Simak J.; Hall J. B.; Semberova J.; De Paoli Lacerda S. H.; McNeil S. E. *Mol. Pharmaceutics* **2012**, 9(3), 382–393. doi: 10.1021/mp200463e

7.  Jones C. F.; Campbell R. A.; Franks Z.; Gibson C. C.; Thiagarajan G.; Vieira-de-Abreu A.; Sukavaneshvar S.; Mohammad S. F.; Li D. Y.; Ghandehari H.; Weyrich A. S.; Brooks B. D.; Grainger D. W. *Mol Pharm.* **2012**, 9(6), 1599–1611.

8.  Semberova J.; De Paoli Lacerda S. H.; Simakova O.; Holada K.; Gelderman M. P.; Simak J. *Nano Lett.* **2009**, 9, 3312–3317.

9.  Bihari P.; Holzer M.; Praetner M.; Fent J.; Lerchenberger M.; Reichel C. A.; Rehberg M.; Lakatos S.; Krombach F. *Toxicology* **2010**, 10; 269(2-3);148-54. doi:10.1016/j.tox.2009.08.011

10. De Paoli Lacerda S. H.; Semberova J.; Holada K.; Simakova O.; Hudson S. D.; Simak J. *ACS Nano* **2011**, 5(7), 5808–5813. doi:10.1021/nn2015369

11. Holzer M.; Bihari P.; Praetner M.; Uhl B.; Reichel C.; Fent J.; Vippola M.; Lakatos S.; Krombach F. *J Appl. Toxicol.* **2014**, 34(11), 1167-76. doi 10.1002/jat.2996

12. Khandoga A.; Stoeger T.; Khandoga A. G.; Bihari P.; Karg E.; Ettehadieh D.; Lakatos S.; Fent J.; Schulz H.; Krombach F. *J. Thrombosis Haemostasis* **2010**, 8, 1632–1640. doi: 10.1111/j.1538-7836.2010.03904

13. Khandoga A.; Stampfl A.; Takenaka S.; Schulz H.; Radykewicz R.; Kreyling W.; Krombach F.; *Circulation* **2004**, 109, 1320–1325. doi:10.1161/01.CIR.0000118524.62298.E8

14. Corbalan J. J.; Medina C.; Jacoby A.; Malinski T.; Radomski M. W. *Int. J. Nanomed.* **2012**, 7, 631–639.

15. Napierska D.; Thomassen L. C.; Rabolli V.; Lison D.; Gonzalez L.; Kirsch‑Volders M.; Martens J. A.; Hoet P. H. *Small.* **2009,** 5(7), 846-853. doi:10.1002/smll.200800461

16. Gazzano E.; Ghiazza M.; Polimeni M.; Bolis V.; Fenoglio I.; Attanasio A.; Mazzucco G.; Fubini B.; Ghigo G. *Toxicol. Sci.* **2012,** 128, 158-170.

17. Marucco A.; Gazzano E.; Ghigo D.; Enrico E.; Fenoglio I. *Nanotoxicology* **2016,** 10(1), 1-9.

18. Fenoglio I.; Fubini B.; Ghibaudi E.; Turci F. *Adv. Drug Deliver*. Rev. **2011**, 63, 1186-1209.

19. Marucco A.; Turci F.; O' Neill L.; Byrne H. J.; Fubini B.; Fenoglio I. *J. Coll. Interf. Sci.* **2014**, 419, 86-94.

20. Kokalari I.; Gassino R.; Giovannozzi A. M.; Croin L.; Gazzano E.; Bergamaschi E.; Rossi An. M.; Perrone G.; Riganti C.; Ponti J. Fenoglio I. *Free Radic. Biol. Med*. **2019**, 134, 165-176.

21. Stöber W.; Fink A.; Bohn E. *J. Colloid Interf. Sci.* **1968**, 26(1), 62-69.

22. Monopoli M.; Walczyk D.; Campbell A.; Elia G.; Lynch I.; Baldelli Bombelli F.; *J. Am. Chem. Soc.* **2011**, 133 (8) 2525-2534.

23. Ralph A.; Somers M.; Cowman J.; Voisin B.; Hogan E.; Dunne H.; Dunne E.; Byrne B.; Kent N.; Ricco A. J.; Kenny D.; Wong S. *Cardiovasc Eng. Tech.* **2016,** 7(4), 389–405. doi: 10.1007/s13239-016-0282-x

24. Cowman J.; Richter L.; Walsh R.; Keegan N.; Tinago W.; Ricco A. J.; Hennessy B. T.; Kenny D.; Dunne E. *Platelets* **2019**, 30(6), 737-742

25. Dunne E.; Qi Q. M.; Shaqfeh E. S.; O'Sullivan J. M.; Schoen I.; Ricco A. J.; O'Donnell J. S.; Kenny D. *Blood* **2019**, 133(12), 1371-1377.

26. Pietroiusti A.; Massimiani M.; Fenoglio I.; Colonna M.; Valentini F.; Palleschi G.; Camaioni A.; Magrini A.; Siracusa G.; Bergamaschi A.; Sgambato A.; Campagnolo L. *ACS Nano* **2011**, 5, 4624–4633. doi:https://doi.org/10.1021/nn200372g.

27. Iler R.K., The Chemistry of Silica, Wiley and Sons, New York, 1979.

28. Rimola A.; Costa D.; Sodupe M.; Lambert J. F.; Ugliengo P. *Chem. Rev.* **2013**, 113, 4216−4313. doi: dx.doi.org/10.1021/cr3003054 |

29. McFadyen J.D.; Kaplan Z.S. *Transfusion Med. Rev.* **2015**, 29(2),110-9. doi: 10.1016/j.tmrv.2014.11.006

30. Ruggeri Z.M. *Microcirculation* **2009**, 16(1), 58-83. doi: 10.1080/10739680802651477

31. Jackson S.P. *Blood J.* **2007**, 109(12), 5087-95**.** doi:10.1182/blood-2006-12-027698

32. McFadyen J.D.; Jackson S.P. *Thrombosis Haemostasis* **2013**, 110(5), 859-67. doi: 10.1160/TH13-05-0379.

33. Vroman L.; Adams A. L.; Fischer G.C.; Munoz P. C. *Blood* **1980**, 55, 156-159.

34. Kendall M.; Ding P.; Kendall K. *Nanotoxicology* **2011**, 5(1), 55-65. doi:10.3109/17435390.2010.489724